ELSEVIER

Ceramics International 33 (2007) 655–662

CERAMICS INTERNATIONAL

www.elsevier.com/locate/ceramint

Thermomechanical behavior of a zircon–mullite composite

M. Hamidouche [a], N. Bouaouadja [a], R. Torrecillas [b], G. Fantozzi [c,*]

[a] *Laboratoire des Matériaux Non Métalliques, département d'Optique et de Mécanique de Précision, Université Ferhat Abbas, 19000 Sétif Algérie, France*

[b] *INCAR, Oviedo, Spain*

[c] *Laboratoire GEMPPM, INSA 20 Ave A. Einstein, 69621 Villeurbanne Cedex, France*

Received 14 March 2005; received in revised form 15 October 2005; accepted 12 December 2005
Available online 3 March 2006

Abstract

A zircon–mullite composite was made by reaction sintering from a mixture of mullite and zircon powders. The thermomechanical characterization (strength and toughness) revealed an intermediate behavior between mullite and zircon. The composite presents a high cooling thermal shock resistance for temperatures between the ambient and 1000 °C. Bending creep tests were made at temperatures between 1100 and 1300 °C using stresses from 10 up to 90 MPa. The stress exponent value is between 2 and 3 while the activation energy varies from 280 up to 900 kJ mol^{-1} between 1000 and 1300 °C. Microscopic observations suggest an intergranular creep mechanism. The grain interface forces between mullite and zircon are more important than those of zircon–zircon grains. The incorporation of mullite particles in a zircon matrix produces a composite that has both the good mullite behavior toward creep and the high thermal shock resistance of zircon.

Keywords: C. Creep; C. Thermal shock resistance; D. Mullite; Strain and rupture; Zircon

1. Introduction

Zircon ($ZrSiO_4$) is the only zirconium silicate in the ZrO_2–SiO_2 diagram. It is an abundant and economical ceramic that has a good chemical stability at the ambient and high temperatures up to 1667 °C where the zircon dissociation onto zirconia and silica occurs [1]. This stability gives a good corrosion resistance to the material. Its low dilatation coefficient makes it very resistant to thermal shock [2]. However, its low creep resistance limits its application.

Garvie [3] was the first to study zircon reinforcement (toughening) by zirconia. He demonstrated the positive effect of adding ZrO_2 on the zircon mechanical properties. He showed that $ZrSiO_4$ and ZrO_2 were mutually compatible on all proportions up to the zircon dissociation temperature. The major effect of adding zirconia is the improvement of the composite thermal shock resistance. The author concluded that the reinforcement was possible because of crack deviations and branching. Ying [4] studied the influence of adding a 20% volume of stabilized zirconia (Y-TZP) in a zircon matrix. A 40% toughness and a 20% strength increases were recorded. Microstructural observations showed that the Y-TZP addition induces an inhibition of the zircon grain growth during sintering. This inhibition is caused by the presence of intergranular zirconia. DRX analysis confirmed the T-ZrO_2 → M-ZrO_2 transformation and the microcracking toughening mechanism. Kondoh [5] was particularly interested in the consequences of adding a 20% volume of SiC whiskers to a zircon matrix. In comparison to monolithic zircon, the fracture stresses for three grades that were studied were much higher. These were inversely proportional to the fibers size. Kondoh [5] explains the improved characteristics of the SiC whiskers–zircon composites by the presence of residual stresses. These are caused by the difference in the dilatation coefficients of the SiC whiskers and the matrix. However, the low strength of large fibers reduces the composite mechanical strength. At high temperatures (>1100 °C), the strength deterioration is due to subcritical crack growth and mechanisms controlling the monolithic zircon fracture. The usually known creep mechanisms in such ceramics are the grain boundary sliding and the formation and coalescence of cavities. In another work, Zhen-Yan Deng [6] showed that the addition of a 20% volume of SiC or TiC particles into a zircon matrix, improves the crack propagation resistance. The author noticed a more pronounced

* Corresponding author. Fax: +33 4 72 43 85 28.
E-mail address: gilbert.fantozzi@insa-lyon.fr (G. Fantozzi).

0272-8842/$32.00
doi:10.1016/j.ceramint.2005.12.002

R-curve effect in dispersoidal TiC composites. This toughness increase is explained by the difference between the superficial and bulk residual stresses (indented sample).

The mixings of alumina and zircon powders lead to a formation of mullite–zirconia composites after sintering [7,8]. Usually in the case of dispersoidal composites, the mullite component is used as a matrix [9,10]. But in the present work, the mullite is incorporated as a reinforcement agent into a zircon matrix ($ZrSiO_4$) by reaction sintering. Mullite has very good thermomechanical properties [9].

Our objective is to study the thermomechanical behavior of a zircon ceramic reinforced with mullite. A comparison with the behavior of related materials, like monolithic mullite and zircon, is made.

2. Experimental procedure

The zircon–mullite composite was made by reaction sintering from a mixture of alumina and zircon powders. The mass proportions were 90% and 10% for zircon and alumina, respectively. The mixture was kneaded in a propyl alcohol solution for 30 min using a zircon balls grinder. After drying, slabs of dimensions (25 mm × 25 mm × 5 mm) were prepared by isostatic compression under a pressure of 200 MPa. The sintering operation was carried out at a temperature of 1560 °C for 2 h. In order to increase the amount of mullite precipitated from the vitreous phase, an annealing treatment for 8 h was made at a temperature of 1450 °C. Samples of dimensions (40 mm × 6 mm × 4 mm) were obtained after cutting and adjusting operations.

The microstructure was observed under a scanning electronic microscope (JEOL JSM 840 A LGS). The samples were surface ground with emery paper (600 and 1000 grits) and polished with 1 μm diamond pastes on padded rotating disks [9]. The surface polishing was controlled visually (mirror like surface). In order to bring out the presence of grain boundaries, an annealing type treatment was made at a temperature of 1400 °C for 1 h. A surface metallization with a thin gold layer was made by vacuum evaporation to assure electronic conduction.

The Young's modulus was evaluated as a function of temperature using a dynamic method (GRINDO SONIC). The mechanical strength was determined by four-point bending on an INSTRON testing machine, using a displacement rate of 0.5 mm/min. The upper and lower supports of the four-point bending rig are, respectively, 10 and 35 mm. The strength was evaluated according to the following relation [9]:

$$\sigma_f = \frac{3P_r(L-l)}{2BW^2} \quad (1)$$

P_r: fracture load; L, l: distances between lower and upper supports (35 and 10 mm respectively); B: sample width; and W: sample thickness.

The toughness determination was made on single edge notched beam (SENB) samples using the same four-point bending rig and under the same conditions as for the strength tests. Samples of dimensions (40 mm × 6 mm × 4 mm) were notched to a depth of 2.4 mm with a diamond saw of 300 μm thickness. Many methods are currently used to measure the fracture toughness of ceramics materials. The single edge notched beam is a simple and inexpensive method that can be influenced by the tip radius of the sawed notch [11]. Other more reliable methods were also proposed [12]. In our case, we used the SENB method to compare to the K_{1C} values obtained for monolothic mullite and monolithic zircon with the same technique [13,14]. We admit that in the tip of the sawed notch of this brittle material there are some microcracks, which are similar to natural cracks.

The toughness relation is:

$$K_{1c} = y\sigma_f\sqrt{a} \quad (2)$$

where "a" is the initial crack length and "y" is a geometric factor corresponding to:

$$y = 1.106 - 1.552\left(\frac{a}{w}\right) + 7.71\left(\frac{a}{w}\right)^2 - 13.53\left(\frac{a}{w}\right)^3 + 14.23\left(\frac{a}{w}\right)^4$$

The strength and toughness tests were made in air at temperatures between the ambient and 1300 °C.

The thermal shock tests were realized using an apparatus developed in our laboratory and described in reference [15]. The different thermal shock necessary steps (samples heating, holding, and cooling and damage control) are automatically controlled. The thermal shock test unfolding is made as follows: the sample, placed in a kiln with a pneumatic jack, is heated to the test temperature. The temperature control is made with a thermocouple positioned near the sample. When the measured temperature reaches the recorded temperature, the sample is maintained in the kiln at that temperature for duration of 10 min. With the use of a transferring jack, the sample is then taken out from the kiln and exposed to a compressed air blowing. The cooling operation is made on the two large sample surfaces (40 mm × 6 mm) for 6 s. Mignard [16] had determined the superficial heat transfer coefficient for this apparatus, which is of the order of 600 ± 80 W/m^2/°C. During the cooling period, acoustic activity is recorded at a cyclic rate of 10 kHz. This corresponds to 60,000 measurements of the acoustic emission amplitude in one test. The acoustic emission results are treated in terms of the maximum amplitude, the emission initial time and the recorded echoes number.

The mechanical strength and the elastic modulus were systematically determined for all thermally shocked samples. A visual control of the cracks is made on each sample. The thermal shock tests were done at temperatures between the ambient and 1000 °C.

Most creep models predict a dependence of creep rate on the temperature, stress, and microstructure according to the relationship:

$$\dot{\varepsilon} = \frac{A_1 D}{kT}\frac{\sigma^n}{d^m} \quad (3)$$

A_1: material constant; D: diffusion constant; k: Boltzman constant; T: absolute temperature; d: grain size; σ: applied stress; m: grain size exponent; n: stress exponent.

The diffusion exponents in Eq. (3) is given by:

$$D = D_0 \exp\left(-\frac{Q}{RT}\right) \tag{4}$$

D_0: constant; R: gas constant; Q: activation energy.

The creep tests were made by four-point bending with supports spans of 18 and 36 mm. The choice of these distances ($L = 36$ mm, $l = 18$ mm), is justified by the fact that in these conditions, $K(n)$ (see relation (6)) shows a little variation with the stress exponent n. The surfaces of the samples were previously polished down to 1 μm finish. The creep tests were done at the following temperatures: 1100, 1200, 1250, and 1300 °C. The maximum initial applied stresses, evaluated by Eq. (1), are within the range (10–90 MPa). The extended use of Eq. (1) in the plastic domain induces less than 5% error in comparison with the use of more complex formulations proposed by Hollenberg [17]. On the other hand, the strain was evaluated, according to the following relations proposed by Hollenberg:

$$\varepsilon = K(n)y \tag{5}$$

y: sample deflection

$$K(n) = \frac{2w(n+2)}{\{(L-1)[(L+1)(n+1)+(n+2)/2]\}} \tag{6}$$

3. Results and discussion

The representative microstructure of the studied material is shown on SEM micrographs in Fig. 1. We noted the presence of three distinct phases: a zircon matrix (ZS) in grey, mullite grains M in darker grey and zirconia grains Z in light grey. Zircon grains have round shape and two types of zircon grains are observed (bimodal grain size distribution): smaller grains (2–5 μm approximately) and larger grains (approximately between 5 and 10 μm). We can notice that the small grains, located in triple points or in mullite conglomerates, are uniformly distributed. The mullite grains, randomly shaped, are located between large zircon grains. The mullite phase distribution is homogeneous. The presence of zirconia grains, confirmed by microanalysis, seem to originate at the beginning of the zircon dissociation. This dissociation usually starts at a temperature of 1670 °C. The presence of impurities in the starting zircon powder (1.2% HfO_2, 0.2% TiO_2, and 0.1% Fe_2O_3) could be at the origin of the lower temperature of dissociation. The materials are obtained by reaction sintering from a mixture of alumina and zircon powders. According to the ternary alumina–silica–zircon diagram, the adding of a small amount of alumina to zircon leads to composition located in the compatibility triangle zircon–zirconia–mullite. During heating, zircon will be in equilibrium with a glassy phase. This glassy phase will be formed at a corresponding invariant point

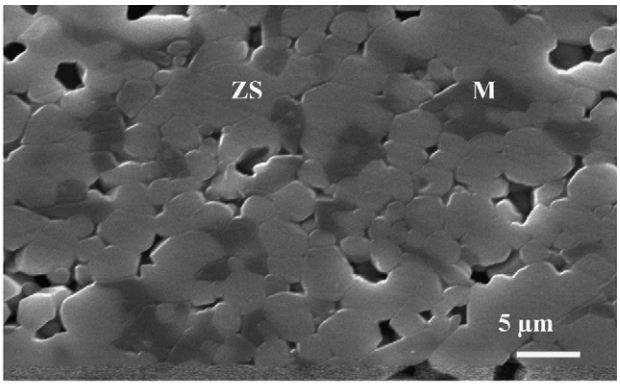

(a)

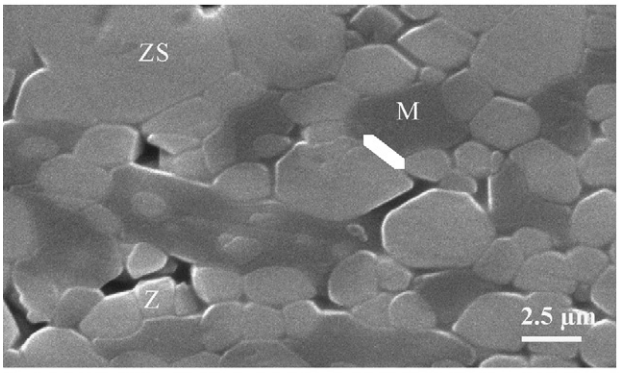

(b)

Fig. 1. SEM micrographs showing: (a) the zircon and mullite phases and (b) smaller zircon grains incrusted in mullite grains.

(around 1450 °C). The alumina present in the mixture will be dissolved in this glassy phase. Mullite is formed from this glassy phase by precipitation during cooling. Some zircon grains are entrapped inside the mullite grains, which have an irregular shape and take the form of the original pores present in the compact. It seems evident that the regions where the zirconia grains are localized are richer in amorphous silica phase. This phase has a significant effect on the mechanical properties of the composite at high temperatures. We noticed that the zirconia is mainly located near porous regions. An important porosity was observed, aside the two main phases previously described, at triple points. Fig. 2 shows a porous

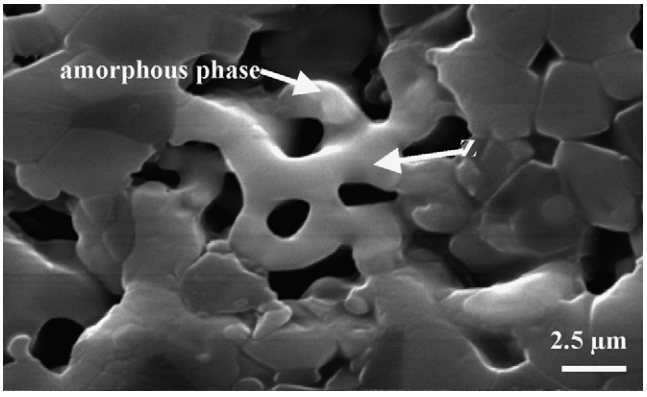

Fig. 2. Zirconia grains localized in the regions witch are richer in amorphous phase.

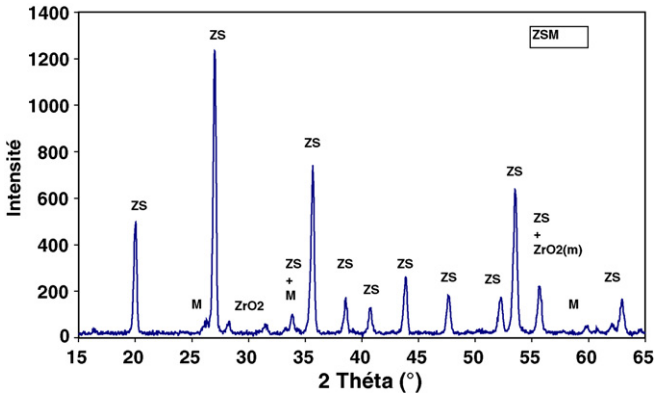

Fig. 3. XRD patterns showing the presence of the phases in the composite (ZS: zircon, M: mullite).

zone rich in vitreous phase with zirconia grains. The XRD patterns (shown in Fig. 3) were established at ambient temperature before thermal shock tests. They confirm the presence of the three phases in the composite.

The measured apparent density (3.88 g/cm^3) by Archimedes' method is less than that of the monolithic zircon. The Vickers hardness average value for this nuance is 11 GPa. It is of the same order than for mullite and zircon [13].

The measured value of the dynamic elastic modulus at the ambient temperature is about 197 GPa. This value is close to the mullite-measured modulus (204 GPa) and lower than that of the zircon value (244 GPa). The high porosity of the composite material is probably the main cause of the low measured modulus in comparison to the two monolithic components. The ZSM composite modulus variation with temperature, shown in Fig. 4, obeys a linear decreasing function defined as: $E_{ZSM} = -0.194T + 197.6$ (T in °C)

The mechanical strength as a function of temperature is represented in Fig. 5. At the ambient temperature, the measured fracture stress is 170 MPa. The strength follows an increasing trend until a maximum (235 MPa) in the temperature range (1000–1100 °C). This evolution can be attributed to the onset of a plasticity caused by the decreasing viscosity of the vitreous phase. At temperatures higher than 1000 °C, the decrease of the viscosity allows grains sliding. This phenomenon generates an important strength drop beyond 1100 °C. It is about 120 MPa at

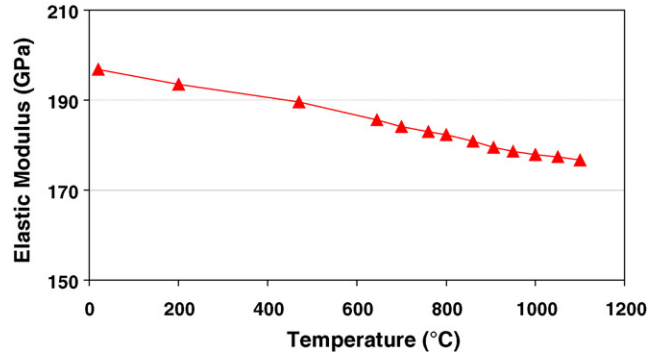

Fig. 4. Evolution of the elastic modulus behavior of zircon–mullite composite as a function of temperature.

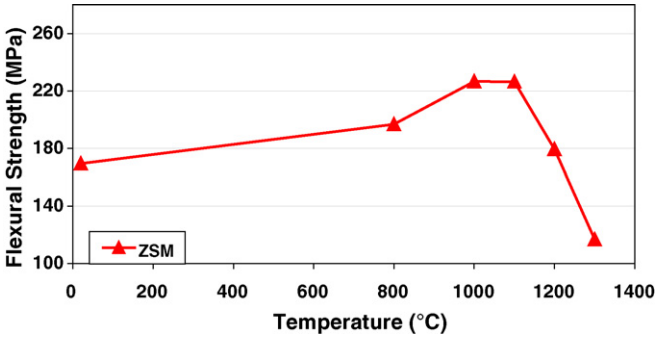

Fig. 5. Bending strength of the composite ZSM vs. temperature.

1300 °C. This represents approximately 30% drop from the strength measured at the ambient temperature.

The ZSM composite fracture toughness K_{IC} measured at ambient temperature is 2 MPa m$^{1/2}$. This value is lower than those of the mullite and the zircon phases, when tested separately [13]. As a function of temperature, K_{IC} increases slightly up to 600 °C (Fig. 6). Above this temperature, an important increase can be noticed. This is also due to the plasticity onset of the vitreous phase. The maximum value (twice the toughness at the ambient) is reached at 1000 °C. Beyond this temperature, a sharp decrease of the toughness is observed. It is caused by the viscosity decrease of the amorphous phase.

The micrographs shown in Fig. 7 represent the crack features of the zircon–mullite composite samples fractured at the temperatures 20 and 1200 °C. We can distinguish between the intragranular and the intergranular types of fracture for, respectively, the ambient and 1200 °C.

For the thermal shock tests, no cracking was observed below a temperature of 950 °C. The corresponding mechanical strengths shown in Fig. 8 do not reveal any appreciable decrease contrarily to dense monolithic ceramics. This confirms the non-damaging effect of the thermal shock up to this temperature. A large dispersion of the measured values is, however, observed. This is directly related to the distribution of the natural flaws present in the material.

The thermal shock behavior of the composite is closely similar to that of the monolithic zircon [13]. An acoustic activity during thermal shock is observed above about 600 °C as shown in Fig. 9. Generally, this acoustic emission appears when there is a released energy during propagation of cracks or

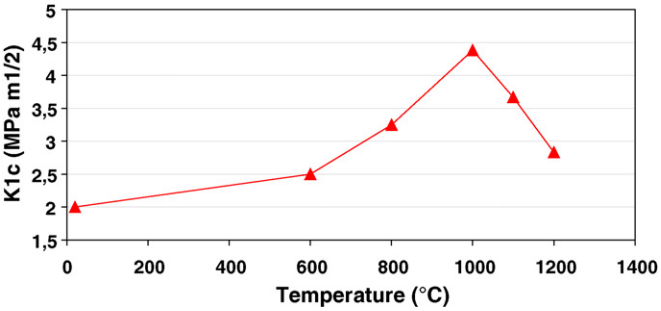

Fig. 6. Fracture toughness K_{IC} determined by SENB as a function of temperature.

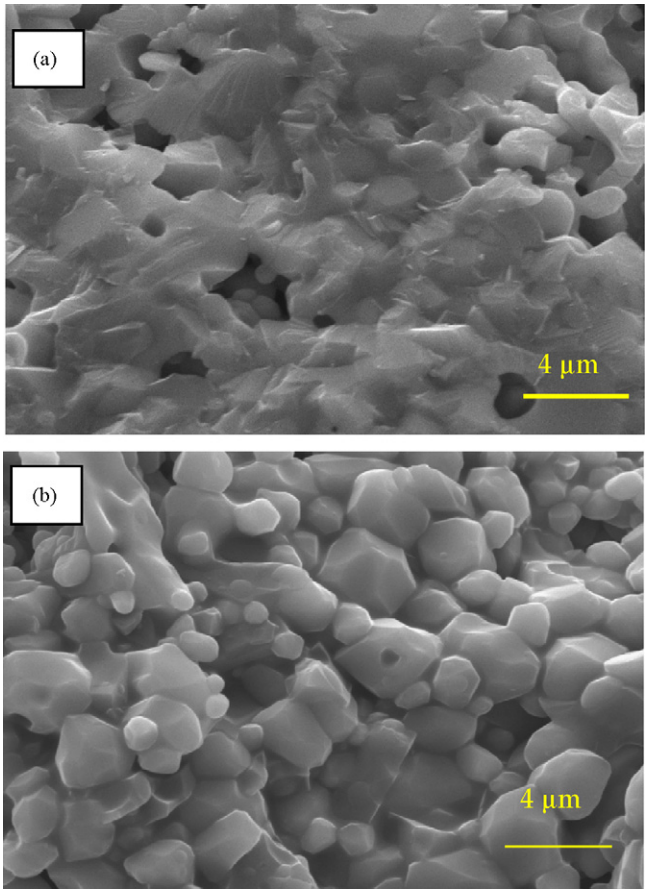

Fig. 7. Micrographs showing the fracture surfaces of the ZSM composite specimens at two temperatures: (a) $T = 20$ °C and (b) $T = 1200$ °C.

during phase transformation. In the case of the present composite, there is no cracking or phase transformation during the thermal shock realized at temperature until 950 °C. So, the acoustic activity observed at temperatures above 600 °C can be caused by the viscosity evolution of the amorphous phase during rapid cooling. During the thermal shock, the amorphous viscosity increases rapidly and grain accommodation occurs relaxing the thermal stresses and inducing acoustic emission activity. As the hot temperature of the thermal shock test

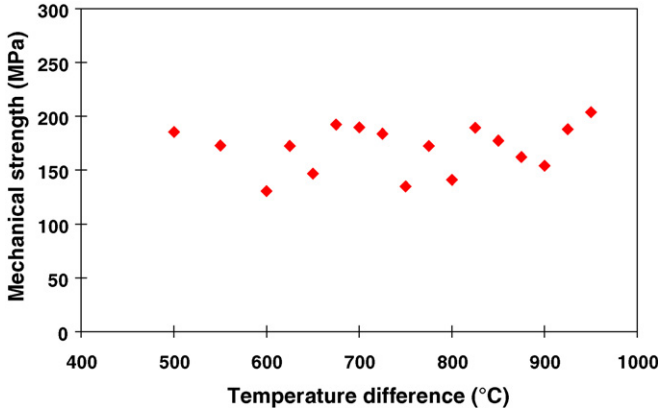

Fig. 8. Mechanical strength of ZSM composite samples subjected to thermal shock as function of the temperature difference ΔT.

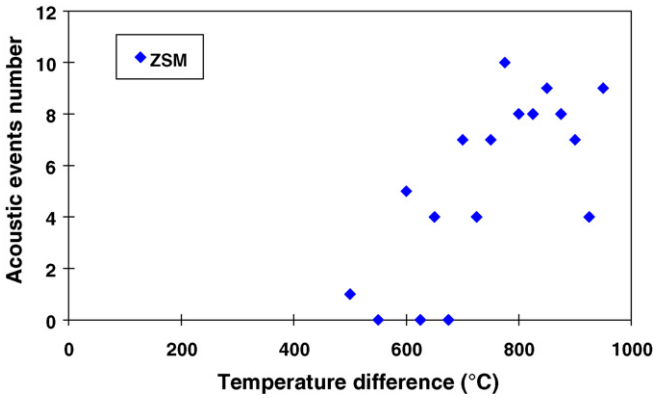

Fig. 9. Evolution of acoustic events with thermal shock temperature difference ΔT.

increases, the recorded acoustic events number increases up to 10 for a temperature of 800 °C.

Fig. 10 shows the creep curves obtained under different stresses at a temperature of 1200 °C. We notice that almost all tests last more than 100 h (with the exception of one sample that failed much sooner at a stress of 90 MPa). All curves show the primary and stationary creep domains. Ternary creep was not observed. The second stage where the strain rate is constant is reached exclusively after a 10-h period for all applied stresses. Similar observations were made at other tests temperatures (1100, 1250, and 1300 °C) for different stress levels.

The strain rate sensitivity to the applied stress is characterized by the stress exponent n. This exponent can be determined by plotting in logarithmic coordinates the variation of the minimal strain rate as a function of the applied stress, as it is shown in Fig. 11. It corresponds to the slope of the straight lines obtained at different temperatures. It increases from the value of 0.98 at 1100 °C, up to 3.02 for 1300 °C. Zircon possesses poor creep resistance due to the presence of a significant intergranular phase [14]. The main creep mechanism is grain boundary sliding (GBS), which is facilitated by the small size and by the rounded shape of the grains. The mullite grain incorporated in the zircon matrix changes the creep behavior. The GBS is prevented by second phase interlocking and glassy phase modification (glassy phase must be reduced or

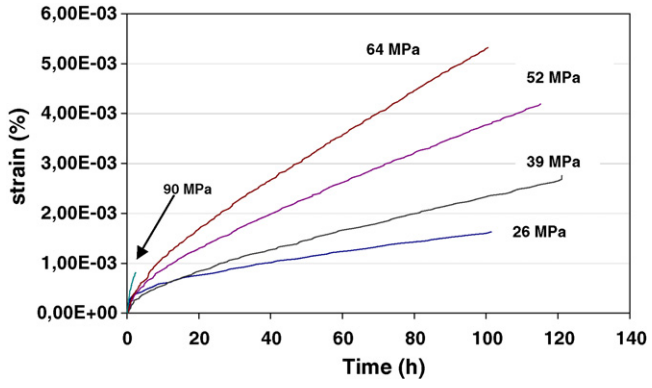

Fig. 10. Creep curves of ZSM samples at 1200 °C with different stresses.

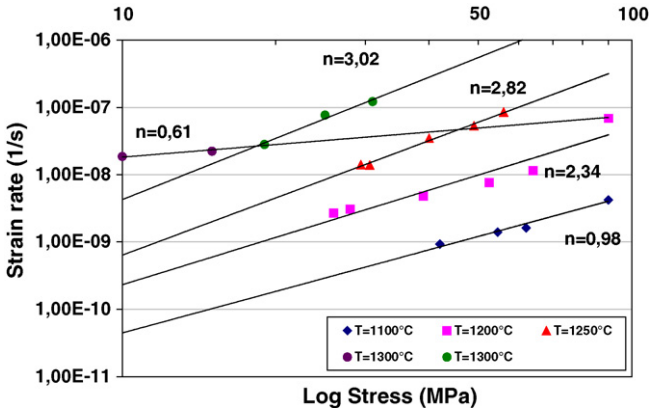

Fig. 11. Strain rate vs. applied stress for different temperatures.

the viscosity modified). The creep resistance of the composite is increased significantly. At low temperature, creep occurs by small grain motion (GBS or rotation), accommodated by viscous creep through the amorphous grain boundary phase. The stress exponent n equal to about 1 confirms this hypothesis [18]. During transient creep, agglomerate accommodation and glassy phase redistribution take place. At high temperatures, the intergranular phase viscosity decreases and the grain motion becomes easier. Cavity formation along the agglomerate boundaries occurs. At high stresses, cavity growth leads to microcrack formation and slow crack growth. Two mechanisms operate in parallel: accumulation of creep damage and slow crack growth. The creep lifetime is limited by slow crack growth, which causes failure during transient creep. This change of creep mechanisms at high temperature leads to a stress exponent n higher than 1 as observed for mullite and zircon [14,18]. It can be noticed that the stress exponent n at high temperatures and at lower stresses is just a little lower than 1, suggesting that GBS accomodated by viscous creep of the amorphous grain boundary phase can occur.

To better understand the creep behavior of the ZSM composite, we made some microscopic observations. We never observed the creep tertiary stages, which means that there was no global damage of the sample. This was confirmed by the absence of macrocracks on the samples (using weak optical magnification). Fig. 12 puts in evidence that an intergranular microcrack growth occurs and that the viscosity of the vitreous phase plays a major role. In this case, the sample fracture takes place by a process of localized damage probably due to the growth of the pores and slow crack growth. The observation of the face in tension of the samples that was crept at 1300 °C revealed that microcracking occurred after creep (Fig. 12). We observed grains boundaries decohesion and cavities coalescence. We also noticed the existence of microcrackings that start from the joints of grains and that meet to form more important cracks. These microcrackings essentially start from the zircon–zircon boundaries. On the other hand, the zircon–mullite interface is more resistant.

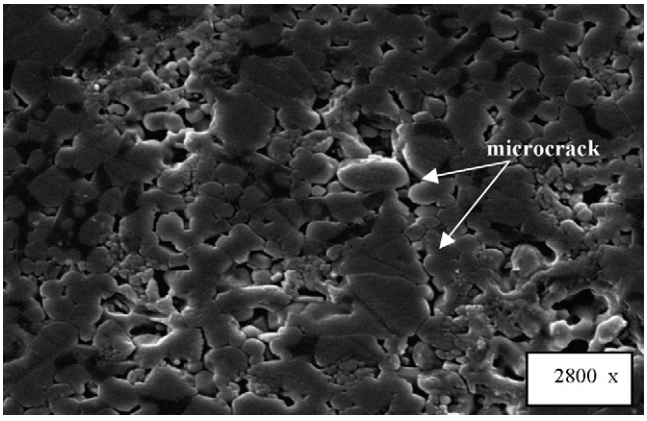

Fig. 12. Micrographs of tensile surface after creep test of 80 h (1300 °C and 31 MPa).

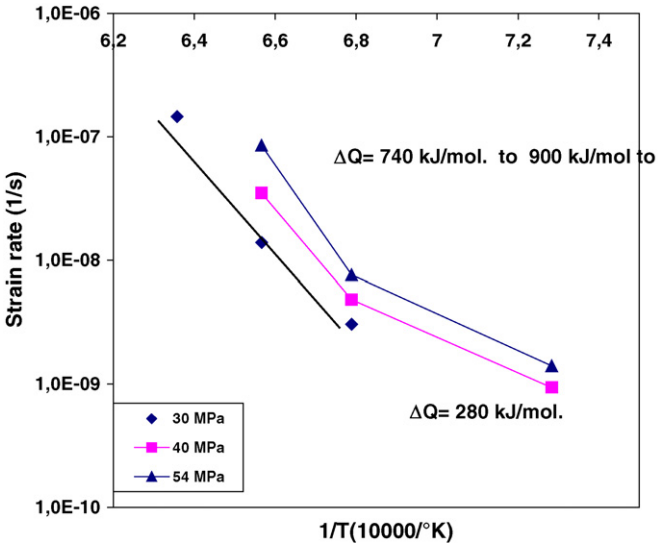

Fig. 13. Strain rate vs. inverse temperature for different stresses.

Creep is a thermally activated process which is given by the general relation (3). The applied activation energy Q can be obtained by plotting the logarithm of the strain rate according to the inverse of the temperature for a given stress (Fig. 13). Q is given by the slope of these curves, for all creep mechanisms. For temperatures lower than 1200 °C, the activation energy is of the order of 280 kJ/mol. In this interval of temperature, the activation energy Q does not depend on the applied stress. On the other hand, for the high temperatures ($T > 1200$ °C), Q seems to depend on stress. It is roughly in the range (740–900 kJ/mol).

The activation energies can be compared to those obtained for mullite [18] and zircon [14]. For these two ceramics, two temperature ranges can be distinguished: under 1200 °C and above 1300 °C. At lower temperatures, the measured activation energy (280 kJ/mol) for the zircon–mullite composite is smaller than those measured for mullite and zircon (410 kJ/mol). This activation energy is linked to GBS with the presence of a glassy phase at the grain boundary as shown by the observed microstructure (Fig. 2). The different values observed for the different materials can be linked to the change of composition of the glassy phase. The increase in activation energy at high temperatures is an indication of a change in creep mechanisms probably caused by the decrease of the

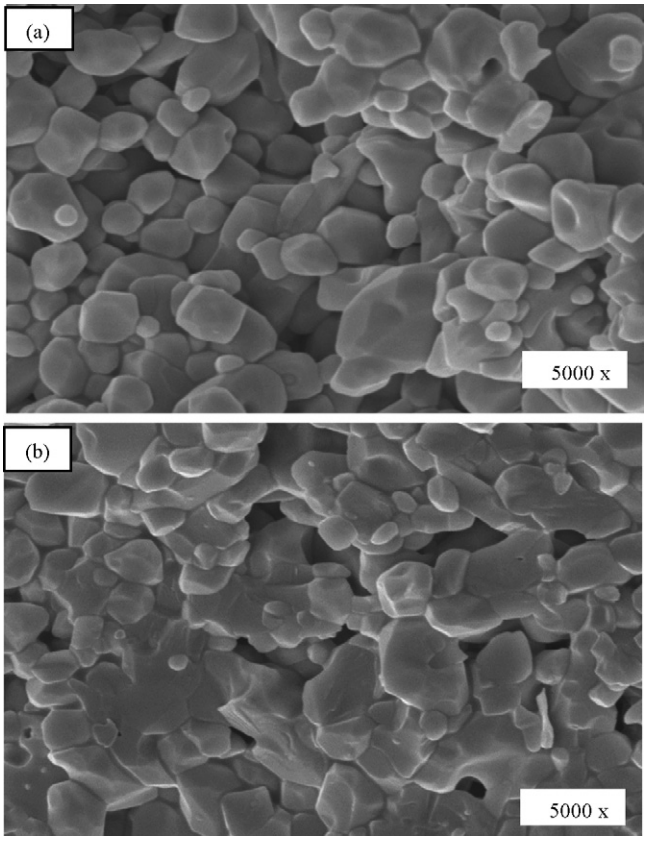

Fig. 14. Fracture surface after creep test ($T = 1300\ ^\circ C$, $\sigma = 31$ MPa) near the tensile (a) and compressive (b) sides.

intergranular phase viscosity, making the grain motion easier. As discussed previously, at high stresses, microcrack formation and slow crack growth occur.

SEM observations of fracture surfaces (after the bending creep test) for the same samples on the compressive and tensile sides (Fig. 14) showed two different zones. Intergranular fracture is predominant on the tensile surface while the fracture is mixed on the compressive side.

4. Conclusion

The analyses of the zircon–mullite ZSM composite revealed the presence of a small quantity of zirconia (ZrO_2), due to a beginning of zircon dissociation. The excess of silica is in the amorphous phase.

The thermomechanical properties of the composite are situated in general between those of mullite M and those of zircon ZS when determined separately.

At ambient temperature, the toughness and the fracture stress of the ZSM composite are lower than those of the monolithic zircon. At high temperature, the tendency is reversed. The elastic modulus remains always lower than those of the monolithic components whatever the temperature.

The thermal shock tests, driven until 1000 °C, showed that this composite did not undergo any cracking. The recorded acoustic activity is related to the relaxation of the thermal stresses due to the change of the viscosity of the glassy phase. The phase change of monolithic zirconia, present in the ZSM composite, is not observed by dilatometry and so, its contribution to the acoustic activity cannot be confirmed.

The good resistance to thermal shock of the ZSM composite can be explained by its better thermoelastic characteristics (thermal conductivity, thermal coefficient of expansion, toughness, ...) relatively to mullite and by the presence of porosity. The damage control by acoustic emission, associated to visual observation, is sufficient for studying the thermal shock resistance of this composite material.

The ZSM creep results showed that the tertiary stage has never been reached. The minimal strain rate is situated between those of two constituents (ZS and M). The stress exponent n is between 1 and 3. The calculated activation energy is of the same order as for the two constituents. The localized damage process takes place by microcracking growth. We noticed that the zircon–mullite interface is stronger.

Knowing the good creep resistance of mullite and the thermal shock resistance of zircon, the results show that the ZSM composite combines the advantages of its two constituents (zircon and mullite).

References

[1] A.W. Timothy, Zircon. From curiosity to commodity, Am. Ceram. Soc. Bull. 68 (5) (1989) 1024–1027.
[2] E.C. Subbarao, D.K. Agrawal, H.A. McKinstry, C.W. Sallese, R. Roy, Thermal expansion of compounds of zircon structure, J. Am. Ceram. Soc. 73 (5) (1990) 1246–1252.
[3] R.C. Garvie, Improved thermal shock resistant refractories from plasma dissociated zircon, J. Mater. Sci. 14 (1979) 817–825.
[4] Ying Shi, Synergistic strengthening and toughening of zircon ceramics by addition of SiC whiskers and 3Y-TZP simultaneously, J. Eur. Ceram. Soc. 17 (1997) 1003–1010.
[5] I. Kondoh, Sintering of zircon-silicon carbide whiskers composites and their mechanical properties, J. Eur. Ceram. Soc. 101 (1993) 358–361.
[6] Zhen-Yang Deng, Effect of residual stress on *R*-curve behaviour of ceramic matrix composites, J. Mater. Sci. Lett. 16 (1997) 977–981.
[7] T. Koya, S. Hayashi, A. Yasumori, K. Okada, M. Schmucker, H. Shneider, Microstructure and mechanical properties of mullite–zirconia composites prepared from alumina and zircon under various firing conditions, J. Eur. Ceram. Soc. 16 (1996) 231–237.
[8] K.A. Khor, Y. Li, Effect of mechanical alloying on the reaction sintering of ZrO_4 and Al_2O_3, Mater. Sci. Eng. A256 (1998) 271–279.
[9] M. Hamidouche, N. Bouaouadja, H. Osmani, R. Torrecillas, G. Fantozzi, Thermomechanical behaviour of mullite zirconia composite, J. Eur. Ceram. Soc. 16 (1996) 441–445.
[10] D. Kaberi, G. Banerjee, Mechanical properties and microstructures of reaction sintered mullite–zirconia composites in the presence of an additive-dispersed, J. Eur. Ceram. Soc. 20 (2000) 153–157.
[11] J. Kübler, Fracture toughness of ceramic using the SEVNB method: preliminary results, Ceram. Eng. Sci. Proc. 18 (4) (1997) 155–162.
[12] J. Kübler, Fracture toughness of ceramics using the SEVNB method: first results for Si_3N_4 of a joint VAMAS/ESIS round robin, Ceram. Eng. Sci. Proc. 20 (3) (1999) 495–502.
[13] M. Hamidouche, Etude de la résistance au choc et à la fatigue thermiques et au fluage des céramiques à base de zircon et de mullite, Thèse de Doctorat d'état, université de Sétif (Algérie), 2002.
[14] X. Carbonneau, M. Hamidouche, C. Olagnon, G. Fantozzi, R. Torrecillas, High temperature behaviour of zircon ceramic, Key Eng. Mater. 132–136 (1997) 571–574.

[15] P. Peigné, Résistance aux chocs thermiques des céramiques thermomécaniques, Thèse de Doctorat, INSA de Lyon, 1991.
[16] F. Mignard, Etude du comportement au choc et à la fatigue thermique de céramiques pour applications industrielles, Thèse de Doctorat, INSA de Lyon, 1994.
[17] C.W. Hollenberg, Calculation of stresses and strain in four point bending creep tests, J. Am. Ceram. Soc. 54 (6) (1971) 196–199.
[18] H. Rhanim, C. Olagnon, G. Fantozzi, R. Torrecillas, Experimental characterisation of high temperature creep resistance of mullite, Ceram. Int. 23 (1997) 497–507.